MICRO/MESOPOROUS COMPOSITES BASED ON COLLOIDAL ZEOLITE GROWN IN MESOPOROUS MATRIX

Pavla PROKEŠOVÁ[a,b], Nikolay PETKOV[a1], Jiří ČEJKA[b1,*], Svetlana MINTOVA[a2] and Thomas BEIN[a3]

[a] *Department of Chemistry, University of Munich (LMU), Butenandtstr. 11 (E), 81377 Munich, Germany; e-mail: [1] n.petkov@ucc.ie, [2] svetlana.mintova@cup.uni-muenchen.de, [3] bein@lmu.de*

[b] *J. Heyrovský Institute of Physical Chemistry, Academy of Sciences of the Czech Republic, Dolejškova 3, CZ-182 23 Prague 8, Czech Republic; e-mail: [1] cejka@jh-inst.cas.cz*

Received June 14, 2005
Accepted July 26, 2005

Composite materials containing micro- and mesopores are prepared under instantaneous hydrothermal treatment of initial solutions generally used for zeolite Beta and precursor solutions for mesoporous Al-MCM-41 material. The resulting composites are compared with pure, highly crystalline colloidal microporous Beta zeolite and hexagonally ordered mesostructured samples. The porosity and morphological features of the composite materials are influenced by the conditions of hydrothermal synthesis of the initial colloidal solutions used for the preparation of Beta seeds, as well as by the conditions of the synchronized crystallization of the final composites. The embedding of Beta seeds in the mesoporous silica matrix is possible via immediate heating of mesoporous precursor solutions with Beta seeds primarily formed. The composite materials contain either microcrystalline Beta nanodomains with sizes of about 5–10 nm surrounded by mesoporous material or defined Beta nanocrystals (20–40 nm), and at the same time connected with mesostructured material. The presence of highly crosslinked silicate framework walls and tetrahedrally coordinated aluminum in the composite material are confirmed by solid-state ^{29}Si and ^{27}Al MAS NMR spectroscopy. The concentration of Brønsted acid sites in the micro/mesoporous composites is increased substantially in comparison with pure mesoporous Al-MCM-41 material proven by FTIR acetonitrile-d_3 adsorption study.

Keywords: Micro/mesoporous composite; Colloidal zeolites; Colloids; Molecular sieves; Acidity; Al-MCM-41; Solid state MAS NMR spectroscopy.

Microporous molecular sieves are widely used as acid catalysts, especially in petrochemical industry[1]. There are many processes, such as alkylations, acylations, disproportionations and isomerizations[2,3], in which these materials replaced conventional and very often not environment-friendly catalysts such as H_3PO_4/SiO_2 or $HCl–AlCl_3$. The main advantages of microporous zeolitic-type materials are their adjustable acidity, size and shape selectivity, high thermal and chemical stability, and environmental toler-

ance[4–6]. Such properties arise from their unique crystalline structure containing regular one-, two- or three-dimensional channel systems of micropores. It is well known that the pore diameter of microporous materials is in the range of 0.2–1.0 nm, which often limits the use of zeolites for reactions involving larger organic molecules than their pore openings. Therefore the active sites in porous crystalline zeolites are accessible only for relatively small organic compounds with a kinetic diameter smaller than 1.0 nm. In order to benefit fully from the unique sorption and shape-selectivity effects in the micropores without suffering from diffusional limitations, the diffusional path length in the micropores should be very short. In zeolite nanocrystals the diffusion paths are a priori shorter, however, they are difficult to handle in practical applications. Prior to application, the nanocrystals have to be embedded into a mesoporous matrix often with irregular pores and low connectivity between zeolite micropores and macropores of the matrix. Then the molecular transport would be inefficient. The ideal pore architecture for molecular transport is that one where short micropores are connected by meso- or macropores going throughout the whole structure. In order to improve the diffusion of both the reactants and products, small nanocrystalline colloidal zeolites have been prepared with large external surfaces due to the nanosized texture of the individual particles forming the samples[7,8].

In contrast to microporous materials, the ordered mesoporous molecular sieves contain larger pores with diameters in the range of 2–50 nm, which could overcome the diffusion and pore size constraints of zeolites. However, the amorphous character of the mesoporous walls entails low hydrothermal and chemical stability and also low acidity that is limiting for their applications in catalysis[9,10].

In order to combine the unique properties of zeolites and mesoporous molecular sieves, micro/mesoporous composite materials have been prepared by several groups[11–13]. Basically, two methodologies exist for the preparation of these materials combining crystalline zeolites and mesoporous molecular sieves[14]. One approach is to prepare mesoporous molecular sieves and then to recrystallize the originally amorphous walls into crystalline zeolitic walls via introduction of an organic template commonly used for synthesis of zeolites[11]. In a similar way the zeolitic template can be added to the reaction mixture before the mesoporous molecular sieves are completely self-organized[12]. The second approach is based on the use of protozeolitic seeds containing small crystalline domains instead of fully crystalline zeolitic particles. These seeds are organized into mesoporous structures using different types of surfactants[13,15,16]. Recently, improved

catalytic activity of the composite materials containing protozeolitic species in comparison with conventional mesoporous Al-MCM-41 material was demonstrated in cumene cracking and toluene alkylation with propene[14]. It was shown, that these properties have arisen from the zeolite-like connectivity of AlO_4 and SiO_4 tetrahedra constructing the walls of framework-type mesostructures.

In our previous works we have shown that micro/mesoporous materials can be prepared via simultaneous reaction of colloidal solutions containing zeolite Beta seeds and mesoporous precursor solutions under hydrothermal conditions[17,18].

The aim of this paper is to study the formation of micro/mesoporous composite materials, i.e., the influence of crystallinity of microporous seeds and the time of immediate hydrothermal treatment on the final particle size and porosity of the composites. The type and concentration of the acid sites for the composites in comparison with pure zeolite Beta and mesoporous Al-MCM-41 materials were investigated based on acetonitrile-d_3 adsorption.

EXPERIMENTAL

Nanosized zeolite Beta samples were synthesized from a colloidal precursor solution having the following chemical composition:

Solution B: 0.35 Na_2O : 9 TEAOH : 0.125–0.25 Al_2O_3 : 25 SiO_2 : 295 H_2O.

The reactants used in the synthesis were freeze-dried silica sol (Ludox SM 30, 30 wt.% in H_2O, Aldrich), aluminum isopropoxide (98%, Aldrich) and tetraethylammonium hydroxide (20 wt.% in water, Aldrich). The as-prepared solution was clear prior to the hydrothermal treatment; the crystallization of pure zeolite Beta was completed within 68 h at 100 °C under static conditions.

The Al-MCM-41 mesoporous material was synthesized from precursor solutions with the following chemical composition:

Solution M: 0.0089 Al_2O_3 : 1 SiO_2 : 19.4 NH_3 : 103 EtOH : 0.28 CTAB : 826 H_2O.

First, surfactant (CTAB, hexadecyltrimethylammonim bromide, Aldrich) and aluminum isopropoxide were dissolved in the solution containing ethanol, ammonia and water, and then tetraethyl orthosilicate (TEOS, 98%, Aldrich) was added at once. Freshly prepared solutions were stirred at room temperature for 24 h resulting in the formation of mesoporous material Al-MCM-41with hexagonal structure.

The micro/mesoporous composites were synthesized from solutions (BM) containing zeolite Beta seeds (solution B) and a freshly prepared precursor solution for mesoporous materials (solution M).

Two synthetic procedures were used to generate the composite materials: (1) heating of solution B for 27 h and, immediately after cooling to room temperature, the solution was mixed with a freshly prepared precursor solution M (Table I, samples BM1a–BM1c). Further crystallization of these solutions was carried out at 100 °C for (up to) 20 h; (2) preliminary crystallization of solution B from 27 to 68 h (Table I, samples BM2a–BM2c), subsequent mix-

ing of solutions B with M, followed by crystal growth of the composite materials at 100 °C for 40 h.

Prior to further characterization, all products from solutions B, M and BM were purified by repeated centrifugation at 20 000 rpm for 1 h, redispersed in doubly distilled water in an ultrasonic bath, and freeze-dried in a Christ Alpha 1-4 vacuum drier overnight in order to prevent further agglomeration of crystalline nanoparticles. Finally, pure zeolite Beta was calcined at 500 °C for 7 h in air flow, while the Al-MCM-41 and micro/mesoporous composites were heated at 550 and 470 °C, respectively, in nitrogen for 1 h, and then in air for 6 h in order to completely remove the organic template (TEAOH) and the surfactant (CTAB).

The four-time repeated ion-exchange of all synthesized materials into the H-form was carried out with 0.5 M ammonium nitrate (100 ml).

The type of the crystalline phase was confirmed by X-ray powder diffraction of the purified and freeze-dried samples in the θ–θ scan mode (Scintag XDS 2000 cooled Ge detector, CuKα radiation). The XRD patterns in the angle ranges 1–10° (2θ) and 5–30° (2θ) were recorded from the powder samples using the slit settings 0.1–0.2–0.5–0.3 and 0.2–0.3–1.0–0.5, respectively. The particle size distributions in the precursor solutions and in the crystalline suspensions were determined by dynamic light scattering (DLS, ALV), while the morphological features were studied with a scanning electron microscope (SEM, Philips XL 40) and high resolution transmission electron microscope (TEM, Jeol 2010, 200 kV). The concentration of Lewis and Brønsted acid sites was determined using adsorption of acetonitrile-d_3 followed by FTIR spectroscopy using a Nicolet FTIR Protégé 460 spectrometer; additional IR investigations of all crystalline samples were performed with a FT-IR Bruker Equinox spectrometer. The porosity of the samples was monitored by nitrogen sorption measurements using a Quantachrome Corporation NOVA 4200. The ^{29}Si and ^{27}Al MAS NMR experiments were carried out using a Bruker DSX Avance 500 spectrometer. The chemical composition of the products was determined by inductively coupled plasma atomic emission spectrometry (ICP-AES) using a Varian Vista ICP-AES spectrometer.

TABLE I
Conditions for the preparation of micro/mesoporous composites

Material	Solution B: τ_{cryst}, h	Solution BM: τ_{cryst}, h
BM1a	27	0
BM1b	27	4
BM1c	27	20
BM2a	27	40
BM2b	30	40
BM2c	68	40

RESULTS AND DISCUSSION

The initial precursor solutions used for synthesis of pure zeolite Beta (solution B) and for the mesoporous material (solution M) appeared clear, while after mixing of the two solutions, a visible precipitation took place resulting in the formation of milky suspensions. The generation of solid particles was followed by DLS of undiluted solutions after one-step purification. Figure 1 shows the particle size distribution curves for the micro/mesoporous composite materials synthesized via synthetic procedures 1 and 2. As can be seen, the particle size distribution curves for composite materials are very

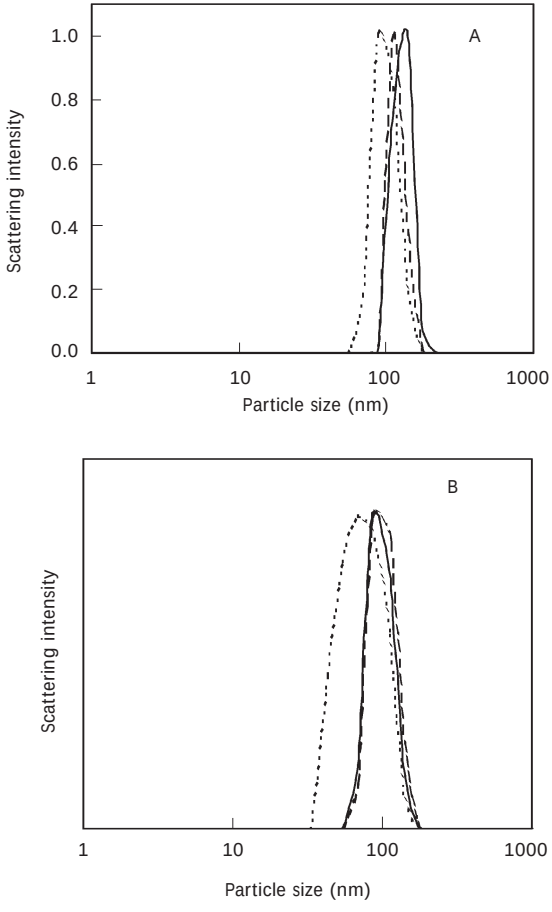

FIG. 1

A: DLS data for micro/mesoporous composites BM1a (——), BM1b (- - -), BM1c (· · ·); B: DLS data of micro/mesoporous composites BM2a (——), BM2b (- - -), BM2c (· · ·)

narrow; the mean particle size decreases from 135 to 90 nm for the composite samples going from BM1a to BM1c (Fig. 1A). However, the particle size distribution in samples prepared via synthetic procedure 2 are broader, and the mean size of the crystals changes from ~120 nm for BM2a to ~70 nm for BM2c samples (Fig. 1B). This implies that solution B with completely crystalline zeolite Beta particles leads to the formation of composite material (sample BM2c) with broader particle size distribution. The pure zeolite Beta nanocrystals have a mean size of about 50 nm and they are smaller than those of the final micro/mesoporous composite (~70–90 nm). For comparison, the mean radius of the pure mesoporous Al-MCM-41 particles is about 290 nm being formed within 10 min under ambient conditions; further stirring of the reaction mixture does not influence the particle size.

In addition to DLS measurements, the size and the shape of all synthesized materials were determined by SEM. Micro/mesoporous composites appeared as a very homogeneous material; no physically isolated phases with different size or morphological appearance were detected. Longer hydrothermal treatment of the synthesis mixture results in the formation of more crystalline and well-shaped spheroidal particles. The composite sample BM2c prepared from a fully crystalline Beta-colloidal suspension containing well-shaped zeolite Beta shows particles that appear very similar to the pure Beta nanocrystals (Fig. 2). The pure zeolite Beta sample contains spheroidal-shaped nanocrystals with well-distinct edges characteristic of crystalline phases (Fig. 2a), while the micro/mesoporous composite samples are shown in Figs 2c–2f. On the other hand, the particles of pure mesoporous Al-MCM-41 material have a broad size distribution and spheroidal or cubic appearance (Fig. 2b).

The crystalline nature of purified and freeze-dried powder samples was demonstrated by X-ray powder diffraction (Fig. 3). The X-ray diffraction pattern of zeolite Beta seeds prepared from solution B at 100 °C for 27 h shows very weak reflections at 6.1, 7.8 and 22.5° 2θ, which are characteristic of polymorph A of zeolite Beta (Fig. 3a). A longer crystallization time leads to more crystalline samples with more sharp and intensive XRD reflections. The XRD pattern of zeolite Beta hydrothermally treated for 68 h contains all characteristic Bragg reflections expected for zeolite Beta (Fig. 3c)[19]. For comparison, the purely mesoporous structure of well-ordered hexagonal Al-MCM-41 is shown in Fig. 3f, and the XRD pattern contains all the Bragg reflections typical of a hexagonal mesoporous material. In contrast to the XRD patterns for pure zeolite Beta (Fig. 3c) and mesoporous Al-MCM-41 (Fig. 3f), the patterns of micro/mesoporous composites (BM1a–BM1c, BM2a–BM2b) show only one reflection in the small-angle re-

gion at about 1.5° (2θ) (Fig. 3e) and very weak reflections characteristic of zeolite Beta at 7.7 and 22.6° (2θ) (Fig. 3d). In the case of sample BM2c, where a milky solution containing fully crystalline zeolite Beta was used as one of the precursors, the XRD pattern contains all reflections characteristic of microporous Beta type material. The intensity of these reflections is approximately 40% of the reflection intensity for pure zeolite Beta sample. This is an indication for the presence of large individual Beta particles in

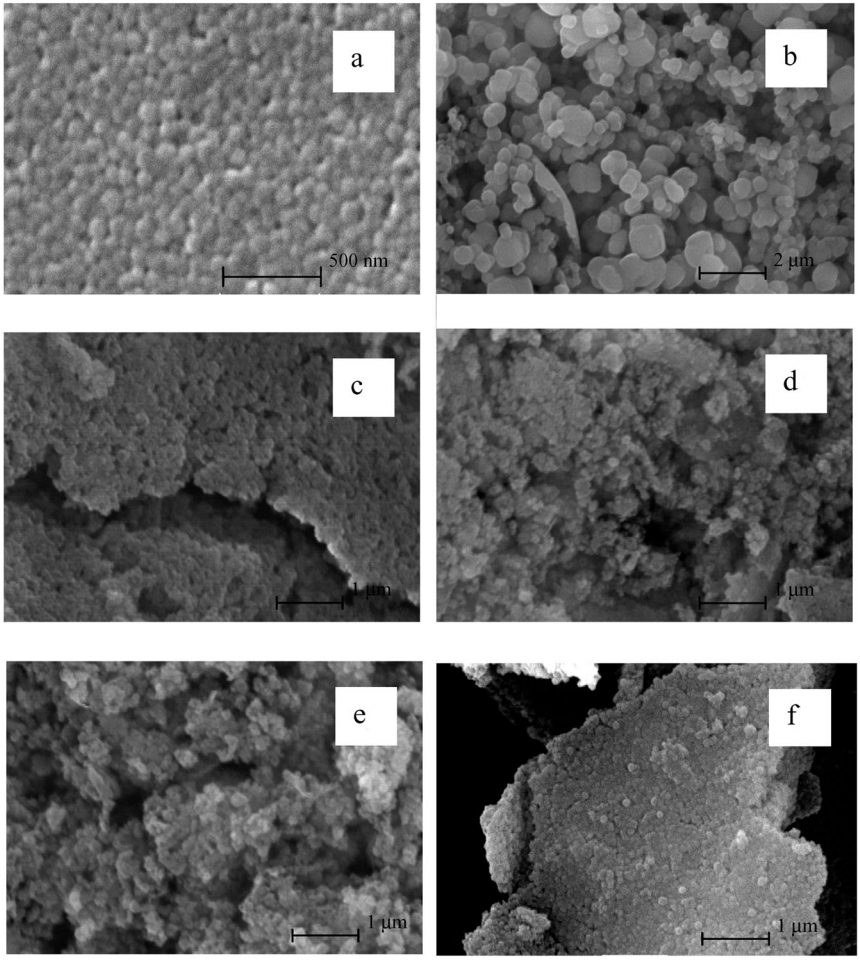

Fig. 2
SEM micrographs of a pure zeolite Beta, b pure mesoporous Al-MCM-41 material, and micro/mesoporous composites c BM1a, d BM1c, e BM2a, f BM2c

the sample BM2c. For sample BM1a, which was not hydrothermally treated after mixing two precursor solutions, the intensity of the reflection at 1.5° (2θ) was very low in comparison with the other micro/mesoporous composite samples, i.e., BM1b–BM1c and BM2a–BM2c. The intensity of all reflections for the calcined samples was higher in comparison with the as-synthesized ones; moreover, no shifts were observed.

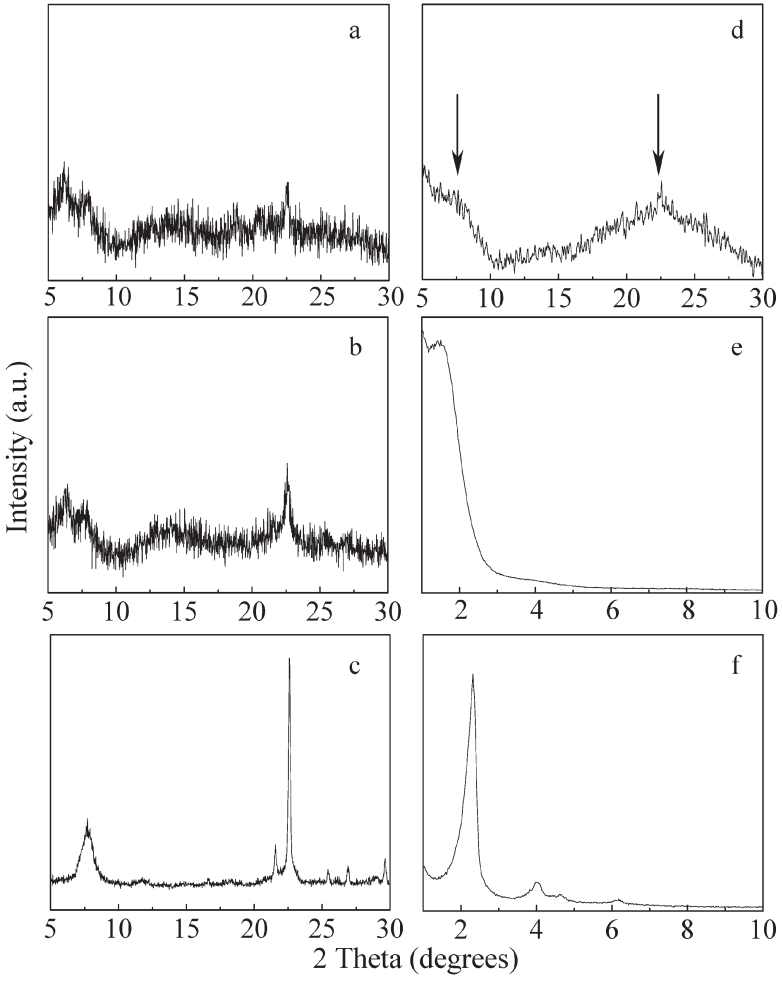

FIG. 3

XRD patterns of samples extracted from solution B heated for a 27 h, b 30 h, c 68 h; micro/mesoporous composite BM1c in the ranges of d 5–30° (2θ) and e 1–10° (2θ), and f pure Al-MCM-41 mesoporous material

In addition, TEM measurements were performed to investigate structural features of the composite materials. Figure 4 shows representative TEM images of pure zeolite Beta crystals and composite materials from samples

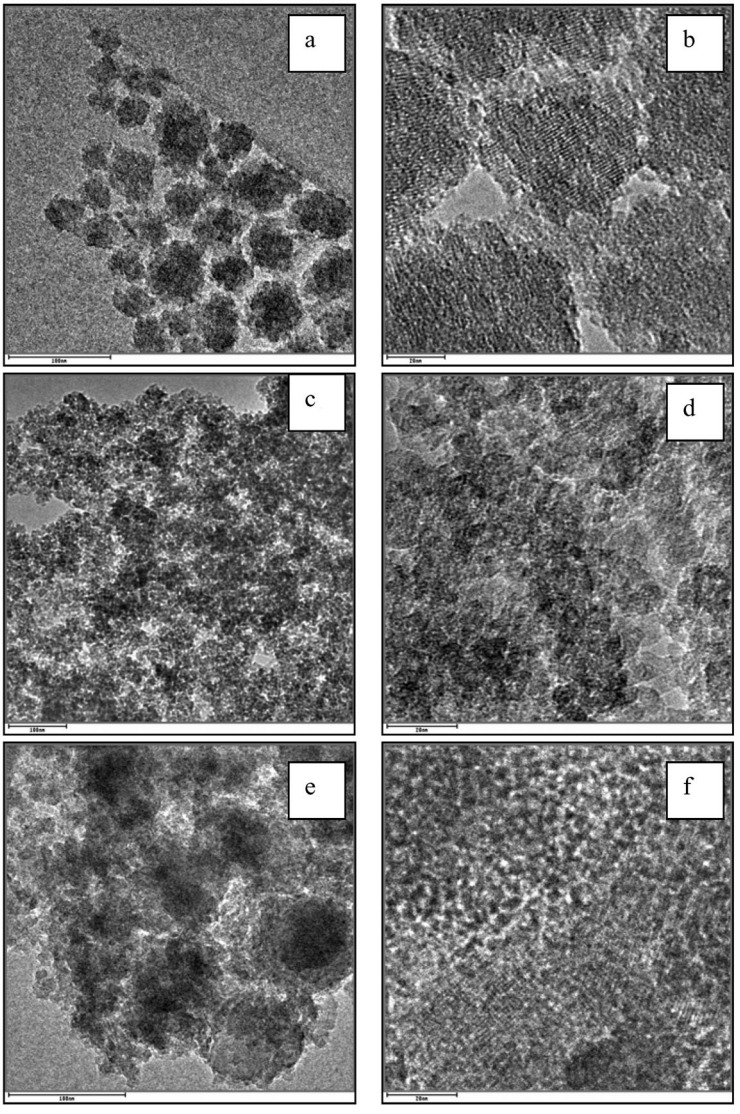

FIG. 4
TEM images of pure zeolite Beta crystals at various magnifications, scale bar size given: a 100 μm and b 20 nm; BM1c composite c 100 nm and d 20 nm; BM2c composite e 100 nm and f 20 nm

BM1c and BM2c after calcination. The pure colloidal Beta particles with size about 50–70 nm are shown in Figs 4a, 4b. The high-resolution TEM images of the pure Beta sample reveal that these particles contain crystalline fringes expected for a BEA-type material, but they are not well aligned within the individual particles. In addition, one could see that these crystals appear rather ridged and probably this is due to the agglomeration of sub-colloidal particles during the drying and calcination processes. However, the different fringes originating from micro- and mesoporous compounds in the composite materials prepared using the first approach are very difficult to be observed in the TEM images (Figs 4c, 4d). One cannot distinguish microcrystalline Beta domains with sizes of ca. 5 nm from mesoporous domains since they are embedded in the mesoporous matrix. In contrast, sample BM2c shows an increased amount of Beta nanocrystals (with dimensions of ca. 20–40 nm), which are closely interconnected through silica matrix with non-ordered mesopores (Figs 4e, 4f). The nanosized Beta crystals are separated and, at the same time, connected through disordered mesostructured matrix giving composite material with well dispersed spatially defined Beta nanocrystals. These results are in a good agreement with the diffraction measurements shown in Fig. 3.

Additional evidence of the presence of pentasil-type zeolite in the micro/mesoporous composite materials is provided by IR spectroscopic data. The vibrational modes between 550–600 cm^{-1} detected in all composite samples (Fig. 5), are due to the presence of five-membered rings as secondary build-

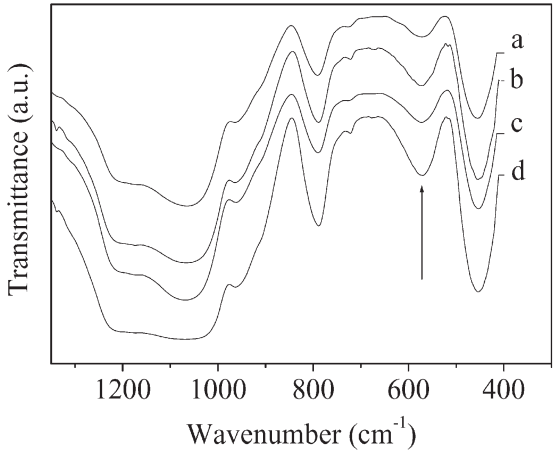

FIG. 5
IR spectra of micro/mesoporous composites of samples a BM1a, b BM1c, c BM2a, d BM2c

ing units in zeolites[20]. Although the XRD patterns of the freeze-dried zeolite Beta samples obtained after short crystallization times (27–30 h) contain low-intensity Bragg reflections, they give rise to a band at 570 cm^{-1}, which is the evidence that a short-range organization exists in the aluminosilicate particles. In the case of fully crystalline zeolite Beta, two distinct bands at 570 and 520 cm^{-1} were detected[17], while in the spectra of micro/mesoporous composite materials only one vibration band at 570 cm^{-1} was recorded (Fig. 5). The latter vibration band was also not observed in the spectra of pure MCM-41 and MCM-48 samples demonstrating the absence of 5-membered rings, which do not apparently exist in pure mesoporous materials.

As it was already indicated on the basis of X-ray powder diffraction, the composite materials possess both micro- and mesoporous features. For comparison, the isotherm of a pure zeolite Beta sample exhibiting inter-particle or the so called textural porosity due to the particle stacking is shown in Fig. 6a. In contrast, the pure Al-MCM-41 material shows distinct adsorption and desorption steps indicating uniform mesopores (p/p_0 ~ 0.3) and no inter-particle porosity (Fig. 6b). However, the specific surface area of pure Al-MCM-41 sample is 1318 $m^2\ g^{-1}$ and the calculated pore diameter based on the Barret–Joyner–Hallenda model is ca. 1.9 nm. In the composite materials BM1b and BM2a, the presence of two types of mesopores is shown (Figs 6c, 6d). The data extracted from the sorption measurements, i.e., total adsorbed amounts of nitrogen, specific surface area and pore diameters calculated from the desorption parts of isotherms for all micro/mesoporous composite samples are summarized in Table II. For composites prepared via synthetic procedure 1, longer crystallization times lead to the formation of samples with higher specific surface areas, i.e. the BET surface areas are about 689 and 969 $m^2\ g^{-1}$ for BM1a and BM1c, respectively. The specific surface areas of the composite materials are between those of typical pure mesoporous materials and pure colloidal microporous Beta type zeolite. The mesopore diameters do not vary significantly in samples obtained for different crystallization times (see Table II). A significant increase in the adsorbed volume of nitrogen at low relative pressures (p/p_0 < 0.12) as well as in the region characteristic for mesoporous material with regular pore system (p/p_0 = 0.25–0.40) is observed for the BM1 series with increasing crystallization time (Table II).

The sorption data collected for samples prepared via synthetic procedure 2 differ from those obtained by procedure 1 discussed above (cf. samples BM2a and BM2b); the pore volume was ca. 20% higher for the BM2-series samples. However, the use of fully crystalline milky suspension of zeolite

Beta (sample BM2c) led to the formation of a composite with a lower specific surface area in comparison with the other samples BM2a and BM2b.

The structure reorganization in the precursor solutions resulting in the formation of composite materials, and in pure Beta and Al-MCM-41 materi-

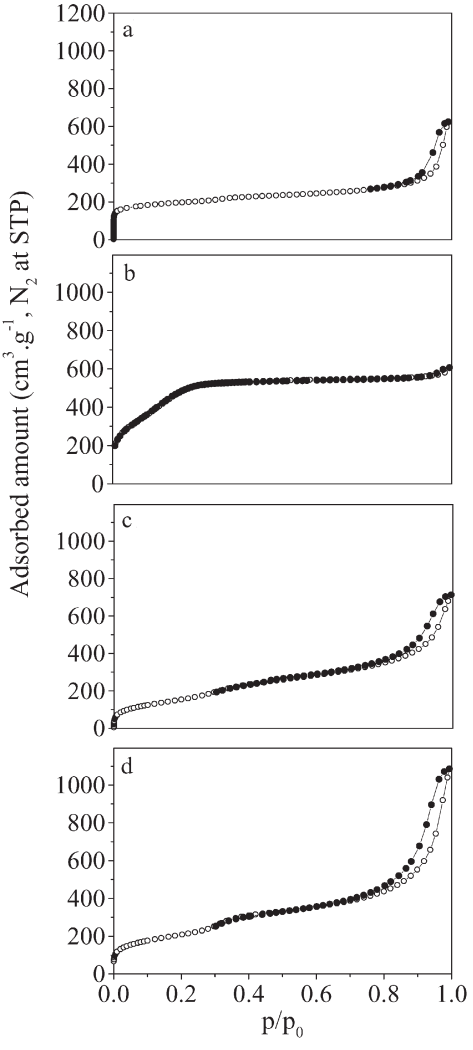

FIG. 6

Nitrogen sorption isotherms of a pure zeolite Beta, b pure mesoporous Al-MCM-41 material, and micro/mesoporous composites c BM1b and d BM2a

als is followed by NMR (Fig. 7). Zeolite Beta seeds prepared from the precursor solution B by hydrothermal treatment for 27 and 30 h, contain both tetrahedrally and octahedrally coordinated Al, occurring at 52–55 and 8–10 ppm, respectively (Fig. 7A, curves a, b). After a certain crystallization time (68 h), the number of Al in octahedral positions decreases and the highly crystalline zeolite Beta samples contain only tetrahedrally coordinated Al (Fig. 7A, curve c). For comparison, the ^{27}Al NMR spectra for the three different materials, pure zeolite Beta, pure Al-MCM-41 and composite BM2a, contain only one peak at 52 ppm characteristic of Al in tehtrahedral position (Fig. 7B). However, calcination of these samples led to a partial transformation of the tetrahedrally into octahedrally coordinated aluminum (Fig. 7C). On the basis of the intensity of the peak at 8 ppm, it can be concluded that the microporous zeolite Beta is very stable under the calcination regime in comparison with the pure mesoporous Al-MCM-41 material. Furthermore, the amount of the octahedrally coordinated aluminum in the composite material is lower compared with the pure mesoporous Al-MCM-41 (Fig. 7C, curves b and c). In addition, solid-state ^{29}Si MAS NMR spectra are collected for the same purified and non-calcined samples. As can be seen in Fig. 7D, the spectra of pure zeolite Beta, pure Al-MCM-41 and the micro/mesoporous composite contain two pronounced peaks between –99 and –109 ppm. In the spectra of zeolite Beta and BM2a composites, the silicon signals are observed at –103.7 and –109.9 ppm, and –101.6 and –109.2 ppm, respectively. The intensity of the peak at –109 ppm is higher compared with the lower-frequency peak for both considered samples i.e. Beta and BM2a (Fig. 7D, curves a and c). The signal at –109.2 ppm arises from Si(4Si), while the peak at –101.6 ppm from connectivity defects attributed

TABLE II
Nitrogen sorption data of micro/mesoporous composites

Material	V_{ads}, cm^3 g^{-1} (p/p_0 < 0.12)	V_{ads}, cm^3 g^{-1} (p/p_0 < 0.99)	ΔV, cm^3 g^{-1} (p/p_0 = 0.25–0.4)	S_{BET}, m^2 g^{-1}	$d_{mesopore}$, nm
BM1a	157	689	45	670	2.4
BM1b	165	762	74	708	2.6
BM1c	182	969	89	747	2.6
BM2a	218	1146	110	915	2.6
BM2b	226	1209	110	911	2.7
BM2c	199	887	65	760	2.7

to Si-OH species and/or to Si(1Al, 3Si). Obviously, the formation of defects is related to the partial removal of Al from the zeolite framework, as has been already detected by ^{27}Al NMR data (Fig. 7C). In contrast to the samples discussed above, the spectrum of the pure mesoporous Al-MCM-41 material contains two peaks at –99.0 and –107.8 ppm, where the former one has higher intensity (Fig. 7D, curve b). On the basis of these results, it can be concluded that the framework walls of micro/mesoporous composite contain highly crosslinked silica species.

As it was shown from electron microscopy and N_2 sorption data, the composite materials possess a high degree of micro- and mesoporosity, and therefore they could be very interesting for further catalytic applications. For that reason, the concentration and the type of acid sites present in the

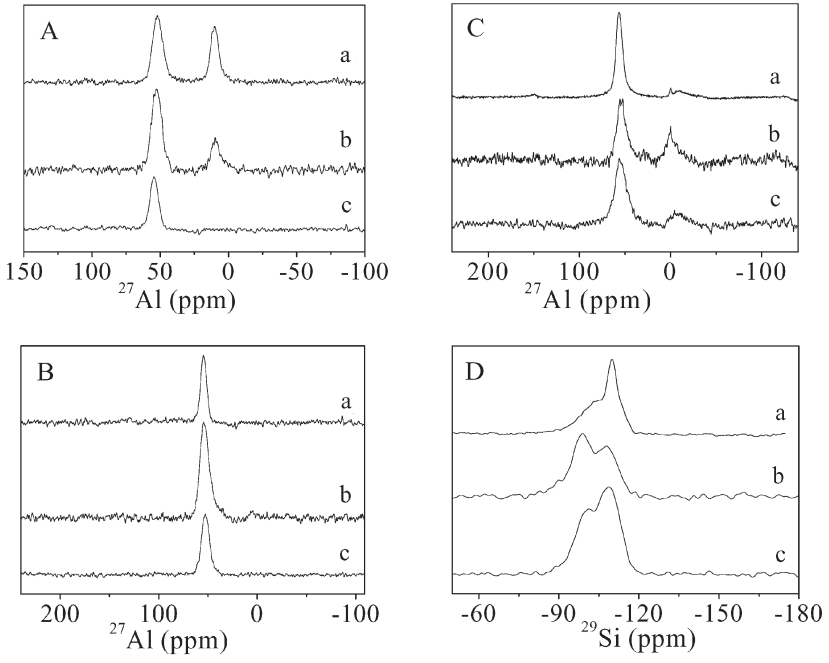

FIG. 7

A: ^{27}Al MAS NMR spectra of Beta seeds after hydrothermal treatment for a 27 h, b 30 h, c 68 h; B: ^{27}Al MAS NMR spectra of as-prepared a pure zeolite Beta, b pure mesoporous Al-MCM-41, and c micro/mesoporous composite (BM2a); C: ^{27}Al MAS NMR spectra of calcined samples of a pure zeolite Beta, b pure Al-MCM-41, and c micro/mesoporous composite (BM2a); D: ^{29}Si MAS NMR spectra of a pure zeolite Beta, b pure Al-MCM-41, and c micro/mesoporous composite (BM2a)

materials were studied using FTIR spectroscopy with acetonitrile-d_3 as a probe molecule. It is well known that zeolite Beta contains a large amount of Lewis sites due to defective three-coordinated Al framework[21]. The coordination of aluminum in the framework of zeolite Beta strongly depends on the conditions of template removal as the stability of aluminum in tetrahedrally coordinated position is rather low.

Figure 8A shows the OH group region in the FTIR spectra of zeolite Beta, Al-MCM-41 and composite material BM2a and BM2c after evacuation at 720 K. A band of terminal silanol groups at 3744 cm^{-1} was found in the spectra of all samples. The FTIR spectra of zeolite Beta and composite material BM2c contain also a typical band characteristic of the bridging OH groups at ca. 3610–3620 cm^{-1} (refs[22–24]). The spectrum of BM2a composite sample contains only a weak band of this vibration.

Adsorption of acetonitrile-d_3 followed by evacuation at 298 K leads to disappearance of the OH band at 3614 cm^{-1} and to a rise in the bands in the region of C≡N bond vibrations (Fig. 8B). The band at 2332 cm^{-1} represents the interaction of the nitrogen atom of the C≡N group of acetonitrile-d_3 with Lewis sites and the bands around 2300 cm^{-1} were ascribed to the interaction of the C≡N group with Brønsted sites[25]. The weaker bands at lower wavenumbers (2260–2280 cm^{-1}) are due to the interactions of the nitrogen atom of the C≡N group with terminal SiOH groups and the acetonitrile-d_3 molecule physisorbed on the sample. The bands at 2300 and 2302 cm^{-1} indicate the presence of Brønsted sites, which are observed in the spectra of pure zeolite Beta and composite BM2c, while only a weak band in the spectrum of the composite sample BM2a is detected (Fig. 8B). This result indicates a higher concentration of Brønsted acid sites in BM2c in comparison with BM2a, due to the presence of large zeolite Beta domains (this has been already detected by TEM, see Fig. 4). Figure 8C shows the results obtained after subtraction of the spectra before and after adsorption of acetonitrile-d_3 for pure Beta, Al-MCM-41 and two composites. The negative bands at 3613, 3614 and 3620 cm^{-1} indicate the presence of Brønsted sites in pure zeolite Beta and in both composite materials, i.e., BM2c and BM2a. Definitely there is not such a band in the spectrum of pure Al-MCM-41 sample (Fig. 8C, curve b).

The concentration of Lewis (LS) and Brønsted acid sites (BS) and the corresponding absorption coefficients were determined from the integral intensity of the C≡N vibrations at 2332 and 2300–2302 cm^{-1} (ref.[25]). Table III summarizes the relative concentration of Brønsted sites ($C_{rel,BS}$ + $C_{rel,LS}$ = 100%), and the Si/Al ratios determined from the FTIR analysis. For comparison, the Si/Al ratio measured by ICP-AES analysis of all crystalline samples

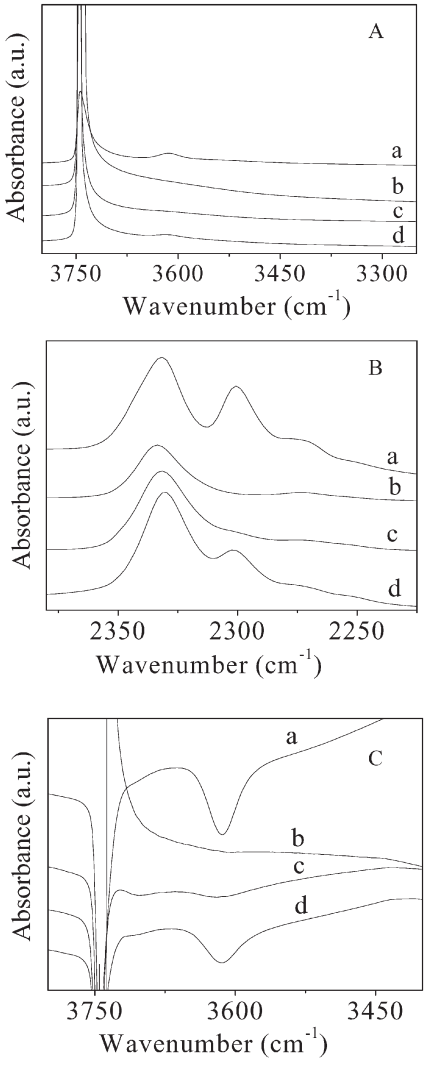

FIG. 8

FTIR spectra of a zeolite Beta, b pure mesoporous Al-MCM-41, and micro/mesoporous composites of c BM2a and d BM2c. A: The spectra are given in the region of 3300–3800 cm^{-1} (evacuated at 720 K overnight); B: The region of the C≡N group vibrations (2200–2400 cm^{-1}) (samples are evacuated at 720 K overnight followed by acetonitrile-d_3 adsorption for 30 min and evacuation for 10 min at room temperature); C: The region of OH groups (3400–3800 cm^{-1}) (subtraction of spectra collected after and before adsorption of acetonitrile-d_3)

is given in Table III. For pure zeolite Beta, the Si/Al ratio calculated from the FTIR adsorption measurements is in good agreement with the result of the ICP chemical analysis. For zeolite Beta with the Si/Al ratio ~33, ca. 46% of all acid sites are of Brønsted type. For pure Al-MCM-41 less than 70% of aluminum in the mesoporous structure is accessible to probe molecules, and there are almost no acid sites of the Brønsted type. This finding was already reported by Dědeček et al.[26] showing that a portion of aluminum is hidden in amorphous walls of mesoporous Al-MCM-41 materials. However, in the composite samples, the concentration of aluminum detected by adsorption of acetonitrile-d_3 was lower in comparison with that determined by chemical analysis, especially for BM2a. This clearly indicates that not all aluminum atoms in the composite material are accessible through the porous system. For BM2c, the concentration of Al determined by the FTIR measurements was much higher than that in BM2a although the concentration of Al in the initial solutions was the same. This is probably due to the use of precursor solutions containing Beta crystals with size of 50 nm instead of Beta seed domain (~5–10 nm) used for the preparation of BM1a–BM1c and BM2a. The relative concentration of Brønsted acid sites is more than twice higher in the case of sample BM2c compared with BM2a, and is very similar to that in pure zeolite Beta (see Table III). FTIR spectra of all materials prepared via synthetic procedure 1 (BM1a–BM1c) are similar to those collected for BM2a. Further experiments showed that with decreasing concentration of Al, the relative concentration of Brønsted acid sites in the structure of micro/mesoporous composite increases.

TABLE III
FTIR and ICP data of pure zeolite Beta, Al-MCM-41 and micro/mesoporous composites

Material	Si/Al ICP-AES	Si/Al FTIR	$C_{rel,BS}$, %
Beta	33	27	46
Al-MCM-41	49	72	1
BM2a	34	40	15
BM2c	31	28	38

CONCLUSIONS

Two different approaches were used for the preparation of micro/mesoporous composite materials via immediate hydrothermal treatment of precursor solutions for pure zeolite Beta and mesoporous Al-MCM-41 type material. Spatially defined Beta nanocrystals connected through the disordered mesostructured matrix were observed in the nano-sized composites obtained by the procedure 2. The long crystallization time for the solutions containing micro- and mesoporous precursors gives more segregated particles with sharp edges similar to those in pure Beta zeolite samples. The presence of highly crosslinked silica framework walls with tetrahedrally coordinated aluminum with enhanced concentration of Brønsted acid sites in the micro/mesoporous composites in comparison with pure Al-MCM-41 was demonstrated. The increased concentration of Brønsted acid sites in the composite was proved by an FTIR acetonitrile-d_3 adsorption study.

Support for this work was provided by the Marie-Curie fellowship, BFHZ and DFG-CNRS. The work of P. Prokešová was also supported by the Grant Agency of the Czech Republic (203/05/0197) and by the Grant Agency of the Academy of Sciences of the Czech Republic (KJB 4040402).

REFERENCES

1. Jacobs P. A., Martens J. A.: *Stud. Surf. Sci. Catal.* **1991**, *58*, 445.
2. Corma A., Martinez A., Arroyo P. A., Monteiro J. L. F., Sousa-Aguiar E. F.: *Appl. Catal.* **1996**, *142*, 139.
3. Čejka J., Wichterlová B.: *Catal. Rev.* **2002**, *44*, 375.
4. Verhoef M. J., Kooyman P. J., van der Waal J. C., Rigutto M. S., Peters J. A., van Bekkum H.: *Chem. Mater.* **2001**, *13*, 683.
5. Weitkamp J.: *Solid State Ionics* **2000**, *131*, 175.
6. Corma A.: *J. Catal.* **2003**, *216*, 298.
7. Botella P., Corma A., Lopez-Nieto J. M., Valencia S., Jacquot R.: *J. Catal.* **2000**, *195*, 161.
8. a) Arribas M. A., Martinez A.: *Catal. Today* **2001**, *65*, 117; b) Mintova S.: *Collect. Czech. Chem. Commun.* **2003**, *68*, 2032.
9. Luan Z. H., Cheng C. F., He H. Y., Klinowsky J.: *J. Phys. Chem.* **1995**, *99*, 10590.
10. Corma A., Grande M. S., Gonzalez Alfaro V., Orchilles A. V.: *J. Catal.* **1996**, *159*, 375.
11. Kloetstra K. R., van Bekkum H., Jansen J. C.: *Chem. Commun.* **1997**, 2281.
12. Poladi R. H. P. R., Landry C. C.: *J. Solid State Chem.* **2002**, *167*, 363.
13. Liu Y., Zhang W., Pinnavaia T. J.: *J. Am. Chem. Soc.* **2000**, *122*, 8791.
14. a) Liu Y., Pinnavaia T. J.: *J. Mater. Chem.* **2002**, *12*, 3179; b) Prokešová P., Žilková N., Mintova S., Bein T., Čejka J.: *Appl. Catal. A* **2005**, *281*, 85.
15. Liu Y., Zhang W., Pinnavaia T. J.: *Angew. Chem., Int. Ed.* **2001**, *40*, 1255.
16. Liu Y., Pinnavaia T. J.: *Chem. Mater.* **2002**, *14*, 3.
17. Prokešová P., Mintova S., Čejka J., Bein T.: *Microporous Mesoporous Mater.* **2003**, *64*, 165.
18. Prokešová P., Mintova S., Čejka J., Bein T.: *Mater. Sci. Eng. C* **2003**, *23*, 1001.

19. Treag M. M. J., Higgins J. B. (Eds): *Collection of Simulated XRD Powder Patterns for Zeolites*, p. 78. Elsevier, Amsterdam 2001.
20. Jansen J. C., van der Gaag F. J., van Bekkum H.: *Zeolites* **1984**, *4*, 369.
21. Bortnovsky O., Sobalík Z., Wichterlová B.: *Microporous Mesoporous Mater.* **2001**, *46*, 265.
22. Kiricsi I., Flego C., Pazzuconi G., Parker W. O., Jr., Millini R., Perego C., Bellussi G.: *J. Phys. Chem.* **1994**, *98*, 4627.
23. Bourgeat-Lami E., Massiani P., Di Renzo F., Espiau P., Fajula F.: *Appl. Catal.* **1991**, *72*, 139.
24. Maache M., Janin A., Lavalley J. C., Joly J. F., Benazzi E.: *Zeolites* **1993**, *13*, 419.
25. Wichterlová B., Tvarůžková Z., Sobalík Z., Sarv P.: *Microporous Mesoporous Mater.* **1998**, *24*, 223.
26. Dědeček J., Žilková N., Čejka J.: *Microporous Mesoporous Mater.* **2001**, *44–45*, 259.